Propagation of tracer signals in boundary currents

Darryn W. Waugh

Department of Earth and Planetary Science, Johns Hopkins University, Baltimore

Timothy M. Hall

NASA Goddard Institute for Space Studies, New York

Submitted to *J. Phys. Oceanogr.*

14 July 2004

Abstract

The propagation of different tracer signals in deep western boundary currents is examined in a simple model in which there is uniform flow in a narrow boundary current and mixing between this current and a stationary interior reservoir. Analytical expressions are derived for the transit-time distributions (TTDs) and for the propagation time ("tracer ages") of tracers with exponentially growing or periodic concentration histories at the boundary current's origin. In the limits of very slow or very rapid mixing between the current and interior reservoir all tracer signals propagate at the same rate: For slow mixing the tracer age equals the advective time, whereas for rapid mixing it equals the mean transit time, which is much larger than the advective time. In contrast, for intermediate mixing rates the tracer age is sensitive to the timescale of the tracer variations (e.g., time constant for exponential growth or period of oscillation), and varies between the advective time and the mean age. Comparisons of the model with CFC and tritium observations indicates that the North Atlantic deep western boundary current (DWBC) is the intermediate mixing regime, with current speed around 5 cm/s and mixing timescale around 1 yr. In this regime anomalies in temperature and salinity of decadal or shorter period will propagate downstream at roughly the current speed, which is much faster than the spreading rate inferred from CFC or tritium-helium ages (e.g., 5 cm/s compared to 2 cm/s). This rapid propagation of anomalies is consistent with observations in the subpolar DWBC, but is at odds with inferences from measurements in the tropical DWBC. The sensitivity of the tracer spreading rates to tracer and mixing timescales in the model suggests that tight constraints on the flow and transport in real DWBCs may be obtained from simultaneous measurements of several different tracers, in particular hydrographic anomalies and steadily-increasing transient tracers.

1 Introduction

Deep western boundary currents (DWBCs) play an important role in ocean circulations and the climate system. In these currents waters formed in polar and subpolar regions flow into other regions, and even the other hemisphere, transporting freshwater and anthropogenic carbon. Quantifying this transport is thus important for understanding the ocean's role in redistributing heat, propagating climate anomalies formed in polar regions, and sequestering anthropogenic carbon.

Estimates of the current speeds and effective transport rates in these boundary currents have been obtained from a variety of measurements, including direct measurements of the velocities, measurements of hydrographic tracers (temperature and salinity) and transient tracers (such as chlorofluorocarbons (CFCs) and tritium), and the movement of subsurface floats. Generally the transport rates inferred from these data differ. For example, the mean velocities in the North Atlantic DWBC from current meters are around 5-10 cm/s (e.g., Watts 1991, Pickart and Smethie 1998), whereas the spreading rates inferred from hydrographic anomalies is 2-2.5 cm/s (e.g., Molinari et al 1998, Freudenthal and Andrie 2002) and that inferred from transient tracer ages is around 1-2 cm/s (e.g., Doney and Jenkins 1994, Smethie et al. 2000, Fine et al. 2003).

It is now recognized that the differences among these estimates are primarily due to mixing and recirculation (e.g., Pickart et al., 1989; Doney and Jenkins, 1994). A wide range of pathways and transit times are available from the surface to points along the DWBC, and the net effect is to reduce the propagation rate of tracer signals below that of pure advection along the DWBC core. However, while past studies have elucidated important aspects of the relationship between tracer propagation and flow, the variety of responses over the full set of available tracers has not yet been fully examined. Two outstanding questions are: Do the signals for tracers with different time dependences propagate at the same rate in DWBCs? If not, how do the differences depend on the balance of advection and mixing? Addressing these questions will, among other things, provide insight into how best to use tracer measurements to infer aspects of the flow and transport in DWBCs.

In this study we examine the dependence of several transient tracers on mixing between the DWBC and the ocean interior using an idealized model in which the DWBC is represented as a narrow advective current that exchanges water and tracer with a much larger stationary reservoir. While similar models have been employed in past DWBC studies (e.g., Pickart et al., 1989; Doney and Jenkins, 1994), our analysis has unique features: (1) We solve explicitly for the transit-time distribution (TTD), which provides a novel framework in which to interpret tracer propagation. (2) We consider a suite of idealized tracers with exponentially- and periodically-varying concentration histories and examine the dependence of the propagation of the tracers on mixing. (3) We apply the model to the propagation of quasi-periodic anomalies in temperature and salinity.

In the next section the model is presented, and compared with several other idealised models used previously. The distributions of transit times in this model are presented and discussed in Section 3. Then in Section 4 idealized tracers with exponential growth or periodic variations are examined. The propagation of realistic tracers (e.g., CFCs and tritium) are examined Section 5, and model results are compared with observations. Concluding remarks are in final section.

2 Model

The model we use consists of two coupled regions: a narrow boundary current with uniform flow u along the current and a larger stationary interior reservoir. Tracers are assumed to be well-mixed in the across-flow direction in both regions. See Fig. 1 for an illustration and Table 1 for a glossary of symbols. There is mixing between the current and interior, which is parameterized as relaxation with timescale t_{mix}. For this system the tracer continuity equations are

$$\frac{\partial \chi_b}{\partial t} + u\frac{\partial \chi_b}{\partial x} + \frac{1}{t_{mix}}(\chi_b - \chi_i) = S_b, \tag{1}$$

$$\frac{\partial \chi_i}{\partial t} - \frac{\alpha}{t_{mix}}(\chi_b - \chi_i) = S_i, \tag{2}$$

where x is the distance along the current, $\chi_b(x,t)$ and $\chi_i(x,t)$ are the tracer concentrations in the boundary current and interior regions, $S_b(x,t)$ and $S_i(x,t)$ are the tracer sources and sinks, and $\alpha = \delta_b/\delta_i$ is the ratio of the width of the boundary current to that of the interior region. Boundary conditions on χ_b are applied at $x = 0$.

This model is highly idealized. In reality the current speed and width, and exchange between current and interior vary both spatially and temporally. Also, in the real oceans there are zonal (across flow) variations in tracers fields and multiple source regions for the tracers. Nonetheless, the model include the features of advective flow in the boundary current and mixing with surrounding regions, both of which are known to be of first-order importance. Moreover, due to it's simplicity, solutions for a variety of tracers are readily obtained and interpreted. Furthermore, as we shall show, the simple model is capable of reproducing many observed features of tracers in the North Atlantic DWBC.

Several other studies have considered similar models. Doney and Jenkins (1994) considered a model the same as that above except that the area of the interior region increased down stream (they expressed the exchange between regions in terms of a coefficient $\kappa = A_b/t_{mix}$, where $A_b = \delta_b L$ is the area of the boundary current). Doney and Jenkins examined the propagation of tritium and excess helium (^{3}He) in this model, but did not present results for other tracers. They presented numerical solutions for a flow configuration with $A_b = 0.8 \times 10^8$ m^2 and A_i increasing from 0.6 $\times 10^8$ m^2 to 2.2 $\times 10^8$ m^2, and showed that the model could reproduce the main features of the observed tritium and excess helium in the North Atlantic DWBC when $u = 5$ cm/s and κ between 1.2 and 2 m^2/s. In terms of the parameters in equations (1) and (2) this corresponds to α between 0.03 and 0.13 and t_{mix} between 1.3 to 2.1 yrs.

Pickart et al. (1989) also considered pipe models of DWBCs (see also Rhein 1994 and Haine et al. 1998). In the models of Pickart et al. there are three regions: an inner advective core, an adjacent shoulder region which exchanges with the core and accumulates tracers, and an infinite surrounding region which is tracer free. Pickart et al. considered two versions, one where the core and shoulder regions have equal cross-section area and there is no motion

in the shoulder region, and another where there is flow in a shoulder region with larger area than the core. Comparisons of CFC measurements in the DWBC near the Grand Banks with both models yielded core speeds of 5-10 cm/s and lateral diffusivities (for mixing between the core and shoulder region) of O(10^6) cm^2 s^{-1}.

The model defined by expressions (1) and (2) is also similar to the "leaky pipe" models used to model transport in the stratosphere (e.g., Neu and Plumb 1999, Hall 2000, Hall and Waugh 2000). The stratospheric leaky pipe models couple a tropical region to two mid-latitude regions, have density decreasing with height (distance along the pipe), and have reverse flow in the mid-latitude regions (constrained by mass continuity). Because of the along-flow density variations the details of the solutions to these models differ from the solutions presented below, but many qualitative features carry over.

We consider here solutions of equations (1) and (2) for several different tracers, including idealised tracers for which analytical solutions can be obtained and realistic tracers for which the solution is obtained numerically by convolution with the analytic transit-time distribution of the model (see next section). Only the solutions within the boundary current are presented in the main body of the text, so we drop the subscript "b". Full solutions for the boundary current and interior are given in the Appendix.

3 Transit-Time Distributions

Several recent studies have highlighted the fact that there is not a single time for transport from one location to another in the oceans but rather a distribution of transit times (e.g., Beining and Roether 1996, Deleersnijder et al. 2001, Khatiwala et al 2001, Haine and Hall 2002). These transit-time distributions (TTDs) correspond to boundary Green's functions that propagate a boundary condition on tracer concentration from a specified region into the interior (Hall and Plumb 1994, Holzer and Hall 2000, Haine and Hall 2002). That is,

$$\chi(x,t) = \int_0^\infty \chi(0, t-\xi)\mathcal{G}(x,\xi)e^{-\lambda\xi}d\xi, \tag{3}$$

where $\chi(0,t)$ is the known tracer concentration history at $x = 0$, and $\mathcal{G}(x,\xi)$ is the propagator, or TTD, with the interpretation that $\delta\xi\mathcal{G}(x,\xi)$ is the mass fraction of the water at x that had last contact with $x = 0$ an elapsed time ξ to $\xi + \delta\xi$. (The factor $e^{-\lambda\xi}$ represents the radioactive decay of the tracer with decay rate λ.) TTDs provide a fundamental description of the transport in a flow, and are independent of any particular tracer.

As outlined in the Appendix the TTDs in the boundary current are

$$\mathcal{G}(x,t) = \hat{G}_1\delta(t - t_{adv}) + \hat{G}_2\Theta(t - t_{adv}), \tag{4}$$

where

$$\hat{G}_1 = e^{-1/Pe}, \quad \hat{G}_2 = \frac{\alpha}{\zeta t_{mix}} e^{-(1+\zeta^2)/Pe} I_1(2\zeta/Pe),$$

$Pe = t_{mix}/t_{adv}$ is the Peclet number, $t_{adv} = x/u$ is the advective timescale, $\zeta^2 = \alpha(\hat{t} - 1)$, $\hat{t} = t/t_{adv}$, I_1 is the modified Bessel function of first order, δ is Dirac delta function, and Θ the Heaviside function. The Peclet number measures the relative importance of advection and mixing within the boundary current, with $Pe >> 1$ for flows dominated by advection and $Pe << 1$ for flows dominated by mixing.

Figure 2 shows TTDs for $t_{adv} = 1$ yr, fractional area of the boundary current $\alpha = 0.1$, and several different mixing times t_{mix} (or equivalently different Peclet numbers). (As it is not possible to plot a literal delta function, the term $\hat{G}_1\delta(t - t_{adv})$ is shown in these plots as a box of width ϵ and height $\hat{G}_1/\epsilon$, with $\epsilon = 0.05$ yr.) If only advection is present the TTD in the boundary current is a delta function at the advective time t_{adv}, i.e., $\hat{G}_1 \to 1$ and $\hat{G}_2 \to 0$ as $t_{mix} \to \infty$. When mixing between the boundary current and interior mixing is added the advective spike is still present but its magnitude is weaker ($\hat{G}_1 < 1$), and there is a "tail" due to water of various ages mixing back into the boundary current (e.g., Fig. 2(a,b)). As the mixing increases (smaller t_{mix} and Pe) the relative contribution due to direct advection in the current decreases ($\hat{G}_1 \to 0$) and the TTD is dominated by older waters that have mixed with the interior (e.g., Fig. 2(c,d)). The TTDs for the interior reservoir are similar but have no advective spike and are shifted to slightly older times (not shown). For different values of α the detailed form of the TTDs differ, but the general shape and variations with t_{mix} are as shown in Fig. 2.

The general shape of the TTDs for this DWBC model is similar to that for the stratospheric tropical leaky pipe (e.g., figure 4 of Waugh and Hall (2002)). Analysis of the stratospheric model shows that inclusion of small or moderate along-flow diffusion results in the δ-function in the TTDs being replaced with finite, narrow peak, without significant change to the resulting tracer solutions (Hall 2000).

The variation of the TTDs in the boundary current with distance downstream is shown in Fig. 3, for $t_{mix} = 1$ yr and $\alpha = 0.1$ (compare with Fig. 2(b)). At all locations the TTDs have an early narrow peak, due to advective transport, and a weak broad tail, due to water that has recirculated through the interior region. The advective peak occurs at later times for larger distances from the source, as it takes longer for the advective flow to reach the location. In the two locations nearest the source the TTDs decrease monotonically for time older than the peak time, but for locations further downstream there is a second, much older, peak in the TTDs. Also, the relative contribution of the advective spike decreases with distance from the source. At 12000 km (approximate distance along the North Atlantic DWBC from the Denmark Strait to the tropical Atlantic) the advective peak at 8 yrs is very small and the TTD is dominated by the tail which has a peak around 70 yrs.

The mean transit time (sometimes called "mean age" or "ideal age") of the boundary current TTD is (see Appendix)

$$\Gamma = t_{adv} \left(1 + \frac{1}{\alpha} \right). \tag{5}$$

The mean transit time Γ is always greater than or equal to the advective time t_{adv}, with $\Gamma >> t_{adv}$ for $\alpha << 1$ (narrow currents). Counterintuitively, Γ is independent of the mixing time t_{mix} despite the fact that TTDs itself is quite sensitive to t_{mix} (Fig. 2). In the interior both the TTD and Γ depend on t_{mix} (Appendix). To understand why Γ in the boundary current is independent of the mixing it is useful to first consider Γ in the interior. The only way the interior region gets new water is through mixing with the boundary current. If the mixing is slow the interior region takes a long time to renew, and Γ in the interior is old. The contribution of mixing of interior water back into the boundary current is then a slow trickle of very old water. Most recent water comes directly from along-stream advection. In

contrast, in the case of rapid mixing there is a shorter renewal time, and younger mean ages, in the interior region. Mixing back into the boundary current then makes a relatively larger contribution. In this model the slow trickle of old water has the same impact as the more rapid flow of younger water, so that the dependence on mixing rate falls out. (Note, this is not the case if there is net divergence in the boundary current, in which case the interior region gets renewed even in the absence of mixing.)

The standard deviation of the boundary current TTD is

$$\sigma = \left(\frac{t_{adv} t_{mix}}{\alpha^2} \right)^{1/2} \tag{6}$$

(The standard deviation $\sigma = \sqrt{2}\Delta$, where Δ is the measure of "width" used by Hall and Plumb (1994) and Waugh et al. (2003).) In contrast to Γ, σ depends on the mixing time t_{mix}. Surprisingly, σ increases for slower mixing. This can be again understood by considering the contribution of mixing of interior water back into the boundary current. As discussed above, for slow mixing most of water comes via advective path with a very small amount of very old water that has been through the interior. However, this small amount makes a very large contribution to σ. In contrast for rapid mixing there is little water via advection and most water has same transit time (which is close to Γ), and the TTD is nearly symmetric about Γ with very small σ (e.g., Fig. 2(d)).

As discussed above the relative importance of advection and mixing is given by the Peclet number, Pe. Using equations (5) and (6), this can be rewritten in terms of the mean and standard deviation of the boundary current TTD:

$$Pe = \frac{t_{mix}}{t_{adv}} = \frac{\sigma^2}{\Gamma^2}(1+\alpha)^2.$$

As Γ is independent of the mixing time but σ increases with mixing time, Pe increases, as expected, with mixing time (i.e. slower mixing).

Several previous studies have used one dimensional flow with constant velocity and diffusion ("1D flow"), or assumed TTDs with the same form as that of 1D flow, when examining differences between transient tracers (e.g., Sonnerup 2001, Wunsch 2002, Waugh et al. 2003), inferring aspects of TTDs from measurements (Klatt et al. 2002, Steinfeldt and Rhein 2004,

Waugh et al. 2002, 2004), and estimating anthropogenic carbon concentrations (Hall et al. 2004, Waugh et al. 2004). It is therefore interesting to compare the above TTDs with those for 1D flow, whose form is sometimes called Inverse Gaussian (IG) (e.g., Seshadri, 1999; and see, Waugh et al., 2003). For weak or intermediate mixing the shape of TTDs in the boundary current model differ significantly from IG distributions. The peak of the boundary current TTDs are are younger and much narrower than those of IG distributions with the same Γ and σ. Also, the boundary current TTD can be bimodal (e.g., Fig. 2(c)) whereas IG distributions are unimodal.

In both the boundary current model and 1D flow the mean transit time is independent of the mixing ($\Gamma = t_{adv}$ for 1D flow) while the standard deviation of the TTD varies with the mixing. However, the two models have very different sensitivities to mixing: The standard deviation increases with mixing in the 1D model ($\sigma^2 = 2\kappa t_{adv}/u^2$, where κ is diffusion coefficient), whereas it decreases with mixing in the boundary current model (see equation (6)). This difference is reflected in the Peclet number: For 1D flow $Pe = 2\Gamma^2/\sigma^2$ (e.g., Waugh and Hall 2002), in contrast to the above relationship where $Pe \propto \sigma^2/\Gamma^2$.

4 Idealised Tracers

Before considering tracers with realistic (observed) boundary conditions we first consider tracers with idealized boundary conditions for which analytical solutions can be obtained directly from equations (1) and (2). Understanding the propagation of these idealised tracers is helpful for understanding propagation of observed tracers.

4.1 Exponential Tracers

We first consider conserved tracers with exponential growth, i.e., $\chi(0,t) = e^{t/T_{exp}}$. Such an increase is a good approximate of the change in CFCs between 1960s and late 1980s (e.g., Pickart et al., 1989). For exponentially increasing tracers analytical solutions for the concentration can be obtained from equations (1) and (2), which can be re-expressed as a

tracer age (see Appendix)

$$\tau_{exp} = t_{adv}\left(1 + \frac{1}{\alpha + r_{exp}}\right), \tag{7}$$

where $r_{exp} = t_{mix}/T_{exp}$. This expression shows that the tracer age is bounded by the advective time and the mean transit time, i.e., $t_{adv} \leq \tau_{exp} \leq \Gamma$. Furthermore, for fixed geometry (α) the ratio of tracer age to advective time depends only on r_{exp}. (An expression of the ratio age of two tracers with different exponential growth rates can also be derived, e.g., Pickart et al. 1989, but we focus here on concentration ages.)

Consider first the limits of large and small r_{exp}. If the mixing time is much longer than the timescale for tracer growth ($r_{exp} >> 1$) then (7) reduces to $\tau_{exp} \approx t_{adv}$, i.e., the tracer age within the boundary current equals the advective time, independent of the tracer growth rate. In this limit new tracer is advected along the boundary current core before mixing with the interior can have any appreciable impact, and the tracer propagation approximates simple bulk advection. In the other limit, $r_{exp} << \alpha$, equation (7) becomes $\tau_{exp} \approx t_{adv}(1+1/\alpha) = \Gamma$. Thus, in the limit of very rapid mixing the tracer age equals the mean transit time (which is much larger than the advective time, for narrow boundary currents), and again there is little sensitivity of the tracer age to the tracer growth rate. In the limit of rapid mixing the TTDs are nearly symmetrical with a relatively narrow peak at the mean transit time (e.g., Fig. 2(d)).

We now consider mixing rates between these two limits. Figure 4 shows the variation of tracer age with mixing time t_{mix}, for several different values of T_{exp} (as in Fig. 2, α = 0.1). In the high and low t_{mix} limits all tracer ages collapse to t_{adv} and Γ, respectively, as discussed above. In between these limits, however, the tracer age varies strongly with timescale for tracer growth. For example, for t_{mix} = 1 yr the age of a tracer with T_{exp} = 7 yrs (approximately the growth timescale of CFC-113 from 1960s to 1980s) is around five times the advective time, whereas the age is around nine times the advective time for T_{exp} = 30 yrs (approximate timescale for CCl_4). The variation of age with mixing and tracer growth for different α is very similar to that shown in Fig. 4. For smaller α there are older tracer ages, especially for weak mixing when the tracer ages tend to the mean transit time,

which is proportional to $(1 + 1/\alpha)$.

As discussed in the Introduction the variation of tracer ages with distance has been used to estimate a spreading rate. From equation (7) we have that the spreading rate of the age of an exponentially increasing tracer is

$$v_{exp} = \frac{\partial x}{\partial \tau_{exp}} = \left(\frac{\alpha + r_{exp}}{1 + \alpha + r_{exp}} \right) u.$$

This shows that (for finite t_{mix}) the tracer spreading rate is less than the core speed, $v_{exp} \leq u$. Also, the tracer spreading rate decreases with increasing r_{exp}. This is illustrated in the upper curves in Fig. 5(a) which show the variation of tracer age with x/u for several T_{exp}, with t_{mix} =1 yr and $\alpha = 0.1$. (If $u = 5$ cm/s then $x/u = 1$ yr corresponds to $x = 1575$ km.) For $t_{mix} = 1$ yr (and measurements in 1990s) the spreading rates of CFC113 and CCl_4 are around $u/5$ and $u/9$, with CFC11 and CFC12 spreading rates between these values.

4.2 Periodic Tracers

Temporal variations (anomalies) in temperature and salinity on decadal and shorter timescales have been observed superposed on longer-term trends in the subpolar and polar North Atlantic. The propagation of these anomalies have been used to estimate transport timescales and spreading rates in the DWBC (e.g., Molinari et al 1998, Freudenthal and Andrie 2002, Stramma et al. 2004). Such anomalies constitute tracers distinct from the steady increase of CFCs (between the 1960s and 1990s). To understand differences between the propagation of these two types of tracers it is useful to consider idealized tracers with periodic boundary conditions, and to contrast them with the exponentially-increasing tracers.

For tracers with periodic boundary condition, i.e., $\chi(0, t) = Re\{e^{i2\pi t/T_\omega}\}$, the propagation time of the phase of the signal (or "phase lag") τ_ω and the relative amplitude A_ω are (see Appendix)

$$\tau_\omega = t_{adv} \left(\frac{\alpha(\alpha + 1) + r_\omega^2}{\alpha^2 + r_\omega^2} \right), \tag{8}$$

$$A_\omega = \exp\left(\frac{-t_{adv} r_\omega^2}{t_{mix}(\alpha^2 + r_\omega^2)} \right) = \exp\left(\frac{-x}{L} \right) \tag{9}$$

where $r_\omega = 2\pi t_{mix}/T_\omega$ is the ratio of the timescales for mixing and tracer variations, and $L = ut_{mix}(\alpha^2 + r_\omega^2)/r_\omega^2$ is the decay length-scale of the amplitude. As with age of exponential tracers, the phase lag is bounded by the advective timescale t_{adv} and the mean transit time Γ, and the ratio of tracer timescale to advective time depends (for fixed α) only on the ratio of timescales for tracer variations and mixing.

If the period of the tracer variation is much shorter than the mixing time, $r_\omega >> 1$, then equations (8) and (9) reduce to $\tau_\omega \approx t_{adv}$ and $A_\omega \approx \exp(-t_{adv}/t_{mix})$ (or $L \approx ut_{mix}$). That is, the tracer signal propagates at the advective speed and amplitude attenuate over a length scale equal to ut_{mix}. TTDs in this limit can still be broad with long tails (see Fig. 2(c,d)), but this tail contributes little to the phase lag. The tail encompasses several complete tracer cycles at roughly equal magnitude, which cancel, and the net signal is due solely to the advective peak. In fact, in this limit, the amplitude of the tracer is equivalent to $\hat{G}_1$, the magnitude of the advective spike of the TTD (see equation 4).

In the opposite limit $r_\omega << \alpha$, the equations (8) and (9) reduce to $\tau_\omega \approx t_{adv}(1+1/\alpha) = \Gamma$ and $A_\omega \approx 1$ (or $L = \infty$). That is, when the tracer period is much greater than the mixing timescale the tracer time lag equals the mean transit time and the amplitude is conserved.

Figure 6 shows the variation of the phase lag and amplitude with mixing time, for several different tracer periods T_ω (again with $t_{adv} = 1$ yr and $\alpha = 0.1$). Consistent with the above analysis, for $t_{mix} > 1$ there is little sensitivity of the phase lag or amplitude to the period of the tracers. For smaller t_{mix} there is some sensitivity, particularly for tracers with periods greater than 10 yrs. However, for t_{mix} around 1 yr and tracers with periods around or less than 10 yrs there is only weak sensitivity, with the phase lag being close to the advective time. Thus, in this regime, the tracer signal downstream of the source will have the same temporal variations as at the source, except lagged by the advective time and smaller amplitude. The weak sensitivity of the phase lag and amplitude to the frequency of the tracer variation means that the propagation of tracer signals are non-dispersive. This is very different from 1-D advective-diffusive flows (and other flows with TTDs similar to IG distributions), where the phase and amplitude vary strongly with the frequency the tracer variations, see, e.g.,

figure 3 of Waugh and Hall (2002).

Figures 5(b) and 6(b) show that for moderate and large mixing ($Pe \leq 1$) there is rapid attenuation of the amplitude of periodic tracers. For example, for the parameters in Fig. 5(b) and current speed $u = 5$ cm/s the amplitude is less than 10% at $x = 4000$ km ($t_{adv} = x/u \approx 2.5$ yrs), and less than 2% at $x = 6000$ km. This means that for these mixing regimes the tracer signal will not be detectable very far downstream from the source region.

The above analysis of the variations of the phase lag and amplitude of periodic tracers suggests that, within the intermediate mixing regime, decadal or shorter variations in temperature or salinity (or other other tracers) will propagate at roughly the advective speed, which is much faster than the propagation of steadily growing (or decaying) transient tracers (such as CFCs). Furthermore, the amplitude of these variations will attenuate very rapidly, and a strong signal is not expected a long way from the source.

5 Realistic Tracers

The above analysis of idealised tracers shows that in the simple boundary current model large differences can exist among the timescales inferred from different tracers. As discussed in the Introduction, differences in tracer timescale (spreading rates) have indeed been noted from observations. To examine this in more detail we now consider the evolution of realistic tracers in the model.

5.1 Transient Tracers

We first consider the distributions of transient tracers CFCs, SF_6, and tritium (^{3}H) and daughter product helium-3 (^{3}He). The concentrations, and ages, of these tracers is determined using equations (3) and (4) together with specified boundary conditions $\chi(0, t)$. For CFCs and SF_6 boundary conditions we use their atmospheric histories (Walker et al., 2000; Maiss and Brenninkmeijer, 1998) scaled to 70% of the equilibrium solubility. This represents typical source conditions of North Atlantic overflow waters (Smethie et al, 2000; Smethie and

Fine, 2001). For tritium the Denmark straight overflow time series from Doney and Jenkins (1994) is used as the boundary condition, and a decay rate $\lambda = 0.05576$ yr^{-1} is used in equation (3). The helium-3 concentration is then calculated as the concentration of tritium lost through radioactive decay (i.e. we consider in the model only helium-3 that comes from tritium decay). The tritium and helium concentrations are then combined together to form a tritium-helium age (e.g., Jenkins and Clarke 1976).

We first compare model distributions of these transient tracers with observations along the North Atlantic DWBC. The symbols in Figure 7 show the observed variations of (a) tritium concentration and (b) tritium-helium age in 1981 (Doney and Jenkins 1994), and (c) CFC11 concentration age and (d) CFC11/CFC12 ratio age in 1991 (Smethie et al. 2000). These observations show that the tritium concentration decreases and tracer ages increase with distance along the DWBC, and that the CFC11 concentration age is significantly older than the tritium-helium age and CFC11/CFC12 ratio age at the same location. (As the CFC11/CFC12 ratio peaked in the mid-1980s the ratio age cannot be defined for the "younger" water in 1991.) The curves in Figure 7 show model calculations for $u = 5$cm/s, $\alpha = 0.1$, and several values of t_{mix}. For $t_{mix} \approx 1$ yrs the model reproduces well the observed variations in all four quantities. Thus, despite its great simplicity, the model is surprisingly good at reproducing the observed tracer signals.

Equally good fits to all four observed quantities is obtained for other values of α, u, and t_{mix}, but the range of values is relatively small. For $\alpha = 0.05$ the data are fit for u around 7 to 9 cm/s and t_{mix} between 1.5 and 0.5 yrs (for slower advection a longer mixing time is required to match the data), whereas for $\alpha = 0.15$ the data are fit for u around 3 to 5 cm/s and t_{mix} between 1.5 and 0.5 yrs. For smaller or larger α it is not possible to match all four quantities simultaneously. The above range of values for u, t_{mix}, and α that result in good agreement between model and observations lies within the "intermediate-mixing" regime, in which the CFC and ^{3}He tracer ages lie between the advective timescale, t_{adv} and the mean transit time, Γ.

The values for both u and t_{mix} are similar to best-fit values in the models of Pickart

et al. (1989) and Doney and Jenkins (1994). Furthermore, the model core velocity in this parameter range ($u \approx 5$ cm/s) is also similar to mean velocities from direct measurements (e.g., Watts 1991, Pickart and Smethie 1998). For the reasons discussed in Section 4, however, $u = 5$cm/s is significantly larger than the tracer-age spreading rates.

We now examine modeled tracer ages in the same mixing regime for a larger suite of tracers. Figure 8 shows the spatial dependence of tracer age (in 1991) for CFC-11, CFC-12, CFC-113, tritium-helium, CCl_4, and SF_6. The model parameter values are $u = 5$ cm/s, $t_{mix} = 1$ yr and $\alpha = 0.1$. The CFC11, CFC12 and tritium-helium ages are similar, except for x greater than about 5000 km, where the tritium-helium age is several years younger than CFC11 and CFC12 ages. The CFC-113 and SF_6 ages are similar to each other, but are younger than CFC11, CFC12, and tritium-helium ages. On the other hand, the CCl_4 age is older than all the other tracers shown. These relationships among the tracer ages hold for other parameters values in the intermediate mixing regime, and are consistent with our analysis of exponentially growing tracers (e.g., Fig. 4).

The range of tracer ages in Fig. 8 is broadly consistent with measurements made in the 1990s of CFCs (Azetu-Scott et al. 2003) and tritium and helium (Khatiwala et al. 2002) in DSOW within the Labrador Sea. Calculations of ages from these observations yield CFC113 ages around 10 yrs, tritium-helium, CFC11 and CFC12 ages around 15 yrs, and CCl_4 ages around 20 yrs. These ages are in reasonable agreement with Fig. 8 for $x = 2500$ km, the approximate distance from the Denmark Strait to the Labrador Sea.

5.2 Hydrographic Tracers

We now consider the propagation of temperature and salinity anomalies. These anomalies act as tracers with fluctuating boundary conditions, and the model analysis of Section 4.2 shows that fluctuating tracers with period less than about 10 years have a timescale for phase propagation closely approximating the advective time, for flow in the intermediate-mixing regime. We therefore expect anomalies in T and S to propagate more quickly along the boundary current than would be indicated by a simple interpretation of CFC or tritium-

helium age.

Dickson et al. (2002) presented long-term salinity time series of overflow waters in the Irminger and Labrador Seas. The major focus of their analysis was the long-term freshening of these waters, but the data also show more rapid variations (oscillations) about this long-term trend. These variations propagate from overflow sills to the Labrador Sea in less than 2 years: For example, the minimum in DSOW salinity at the Denmark Strait in 1994 is observed at the western Irminger Sea in 1995 and in the Labrador Sea in 1996. A 2 year spreading time is consistent with the simple model: It is much shorter than the typical tracer ages in the Labrador Sea of 10 and 20 years (see above), and implies an anomaly spreading rate around 4 cm/s which is close to the mean current speed. Rapid spreading of DSOW temperature anomalies was also observed by Stramma et al. (2004): They noted a propagation time of less than 2 yrs between between the Labrador Sea (56°N) and Grand Banks (43°N), which implies a lower bound on the spreading rate of 3-4 cm/s. This is again broadly consistent with the model.

Temporal variations in temperature and salinity within the subtropical and tropical DWBC have also been reported, e.g., Molinari et al (1998), Freudenthal and Andrie (2002). These studies calculated spreading rates based on anomalies in LSW within the DWBC that are faster than those calculated from tracer ages (2-2.5 cm/s compared to 1-2 cm/s). While this difference between hydrographic anomalies and transient tracer ages is qualitatively consistent with the model, there are quantitative differences for intermediate-mixing parameters. The model-predicted transit time (the advective time) is much shorter than that inferred from the hydrographic observations: assuming a mean current speed of 5 cm/s the time for advection over 6000 km (Labrador Sea to the subtropics) is around 4 yrs, whereas the above studies infer transit times of 8 to 10 yrs. Furthermore the model predicts that the amplitude of the anomalies should be extremely small (e.g., assuming $u = 5$ cm/s and $t_{mix} = 1$ yr the amplitude 6000 km downstream from the source is only about 2% that at the source), whereas the observed tropical anomalies are of similar amplitude to those in the Labrador Sea.

It is possible that these model–data differences are due to the simplicity of the model. The real ocean exhibits temporal and spatial variations in the boundary current's speed, width, and interaction with surrounding waters, processes which are not included in our simple model. However, additional complexity to the flow should generally act to increase, not decrease, the attenuation rate of propagating anomalies. For example, temporal variation in current speed expands the range of transit-times from source to observation point. The transported signal is an average over a wider range of anomaly phases at the source, and its amplitude is further attenuated.

An alternative possibility is that the observed T and S anomalies in the subtropical and tropical DWBC are not simply transported versions of subpolar anomalies, but instead are generated (partially or totally) by variations in ocean circulation. For example, the dynamical variability that produce the T and S anomalies may also affect the transport pathways or generate waves that alter T and S in the tropics (e.g., Yang and Joyce 2003, Johnson and Marshall 2002). Another possibility is that the observed LSW anomalies could be due to local transport features (e.g., eddies), and not related to changes in the source regions.

6 Conclusions

We have examined the transit-time distribution and the propagation of transient tracers in the DWBC using a simple model comprised of a narrow advective core mixing with a stationary reservoir. When there is very rapid or very slow mixing between the current and interior reservoir there is only weak sensitivity of the tracer propagation time (tracer age) to the tracer's concentration history at the source region. In the weak mixing limit the tracer signals propagate at the current speed, whereas in the strong mixing limit the tracer propagation time is close to the mean transit time, which is much older than the advective time. In between these rapid and slow mixing limits the tracer propagation time is, however, sensitive to the concentration history at the source. The propagation time of tracers with exponentially-increasing and periodic histories varies between the advective time and the

mean transit time, depending on the ratio of the tracer timescale (exponential time constant or period of fluctuation) to the mixing time.

Comparisons of the model with CFC, tritium, and helium observations indicates that the North Atlantic DWBC is in the intermediate mixing regime, with current speed $u \approx 5$ cm/s and mixing time $t_{mix} \approx 1$ yr. A current speed of around 5 cm/s is similar to the mean velocities from direct measurements (e.g., Watts 1991, Pickart and Smethie 1998) as well as the values obtained by Pickart et al. (1989) and Doney and Jenkins (1994) for their models. This velocity, however, is faster than spreading rates inferred from CFC and tritium-helium ages, which are around 1-2 cm/s.

For the above parameters the model predicts that the phase of periodic tracers with decadal or shorter periods will propagate at roughly the current speed, and the amplitude of these variations will decay rapidly with distance (e.g., the amplitude at 4000 km downstream is less than 10% that at the source). This implies that decadal or shorter fluctuations in hydrographic tracers (temperature or salinity) will propagate much more quickly than the spreading rate inferred from CFC or tritium-helium ages and that the signal of such variations produced in subpolar regions will have decayed to $\sim 2\%$ in the tropics.

The observed propagation of fluctations in DSOW salinity and temperature in the North Atlantic DWBC are broadly consistent with this model prediction. DSOW salinity anomalies are observed to take less than 2 yrs to propagate from the Denmark straits to the Labrador Sea (Dickson et al. 2000) while DSOW temperature anomalies are observed to propagate from the 56°N and 43°N in less than 2 yrs (Stramma et al. 2004). Both sets of observations imply spreading rates of atleast 3-4 cm/s, which is more rapid than spreading rates from tracer ages and close to the mean current speed. However, transit times inferred from LSW anomalies measured in the (sub)tropical Atlantic (e.g., Molinari et al 1998, Freudenthal and Andrie 2002) are around twice that predicted assuming a current speed of 5 cm/s. In addition, the tropical anomalies have much greater amplitude than predicted by the model. The cause for these differences is unclear. They could be due to deficiencies in the simple model. It is also possible that the anomalies observed in the tropics are not simply

transported subpolar anomalies. Further analysis is need to examine these issues.

A general conclusion from this study is that the impact of mixing on the spreading rate of tracer signals in DWBCs varies among tracers, and a wide range of spreading rates can be obtained from available tracers. This indicates that the tracers contain independent information and suggests that tight constraints on the flow and transport in DWBCs may be obtained from simultaneous measurements of several different tracers, in particular hydrographic anomalies and steadily-increasing transient tracers. We plan to explore this possibility in the future.

One approach for such an analysis is to perform a more detailed model-observation comparison than presented here, including the large database of tracer measurements that now exists from WOCE and other programs. This could involve the current model configuration or more complicated (realistic) configurations (see below). Another approach is to use measurements to constrain aspects (e.g., moments) of the TTDs, without direct reference to a particular transport model. Klatt et al. (2002) and Steinfeldt and Rhein (2004) have performed such an analysis, using repeat CFC measurements to infer the TTDs in the Weddell Sea and tropical Atlantic DWBCs. Caution is required, however, in such an analysis as the results and subsequent interpretation may be sensitive to the assumed shape of the TTDs. The TTDs in the simple model considered here are very different from the Inverse Gaussian functional form used in the above studies (and in Waugh et al. 2004).

As well as the above analysis of observations we also plan to perform further model simulations. Additional features, such as flow in the interior region or time-varying flow parameters, can be included in the model. Analytical solutions are unlikely to be obtained for these more complicated configurations, but solutions can be obtained numerically. An important question to be answered is whether inclusion of additional, more realistic, features in the model dramatically alters the results presented here. In particular, we would like to assess the robustness of our prediction that observed T and S anomalies in the tropics are not simply transported versions of subpolar anomalies. It would also be of interest to examine the issues considered here in dynamical models with more realistic representation of the

processes that exchange fluid between the DWBCs and interior. This may provide not only insight into the transport in DWBCs but also insight into the coupling of the transport to actual physical processes.

Acknowledgments We thank Tom Haine and Toste Tanhua for useful discussions and comments, and Bill Smethie for providing the CFC data shown in Figure 7. This work was supported by the National Science Foundation.

Appendix

The transit-time distributions (TTDs), mean transit time, ages of exponentially increasing tracers, and phase and amplitude of periodic tracers for the model are determined by solving equations (1) and (2) with different sources S_b, S_i and boundary condition $\chi_b(0,t)$.

The TTDs $\mathcal{G}_b$ and $\mathcal{G}_i$ are the solutions of equations (1) and (2) with $S_b = S_i = 0$ and $\chi_b(0,t) = \delta(t)$. These solutions are found by taking the Laplace transform of equations (1) and (2) and then solving a first order differential equation for the Laplace transform of $\mathcal{G}_i$. This yields

$$\begin{aligned} \mathcal{G}_b(x,t) &= \hat{G}_1\delta(t-t_{adv}) + \hat{G}_2\Theta(t-t_{adv}), \\ \mathcal{G}_i(x,t) &= \hat{G}_3\Theta(t-t_{adv}), \end{aligned}$$

where

$$\hat{G}_1 = e^{-1/Pe}, \quad \hat{G}_2 = \frac{\alpha}{\zeta t_{mix}} e^{-(1+\zeta^2)/Pe} I_1(2\zeta/Pe), \quad \hat{G}_3 = \frac{\alpha}{t_{mix}} e^{-(1+\zeta^2)/Pe} I_0(2\zeta/Pe),$$

$Pe = t_{mix}/t_{adv} = t_{mix}u/x$ is the Peclet number in the boundary current, $\zeta^2 = \alpha(\hat{t}-1)$, $\hat{t} = t/t_{adv}$, I_0 and I_1 are modified Bessel function of zeroth and first order, δ is Dirac delta function, and Θ the Heaviside function.

The mean transit time (mean age) of the TTDs is equivalent to the distribution of the ideal age tracer (Hall and Haine 2002). The ideal age tracer is the steady state solution of equations (1) and (2) with $S_b = S_i = 1$ yr/yr and $\chi_b(0,t) = 0$:

$$\Gamma_b = t_{adv}(1 + \frac{1}{\alpha}), \quad \Gamma_i = \Gamma_b + \frac{t_{mix}}{\alpha}.$$

For conserved tracers with exponential growth, i.e., $S_b = S_i = 0$ and $\chi_b(0,t) = e^{t/T_{exp}}$ the concentrations are found using the method of separation of variables. The solutions are then combined with the definition of the tracer concentration age τ, $\chi_b(0, t-\tau) = \chi(x,t)$, to yield

$$\tau_b = t_{adv}(1 + \frac{1}{\alpha + r_{exp}}), \quad \tau_i = \tau_b + T_{exp}\ln(1 + \frac{r_{exp}}{\alpha})$$

where $r_{exp} = t_{mix}/T_{exp}$ is the ratio of mixing to tracer growth timescales.

The solution for conserved tracers with periodic boundary conditions, i.e., $\chi(0,t) = Re\{e^{i2\pi t/T_\omega}\}$, are found in a similar manner. From these solutions it is possible to derive the time lag in phase τ_ω and amplitude A_ω at locations away from the boundary. These are

$$\tau_{\omega b} = t_{adv}\left(\frac{\alpha(\alpha+1)+r_\omega^2}{\alpha^2+r_\omega^2}\right) \quad , \qquad A_{\omega b} = \exp\left(\frac{-\sigma t_{adv} r_\omega^2}{\alpha^2+r_\omega^2}\right)$$

$$\tau_{\omega i} = \tau_{\omega b} + \frac{1}{\omega}\text{atan}(\frac{r_\omega}{\alpha}) \quad , \qquad A_{\omega i} = A_{\omega b} + \frac{\alpha}{\sqrt{\alpha^2+r_\omega^2}}$$

where $r_\omega = 2\pi t_{mix}/T_\omega$ is the ratio of the timescales for mixing and tracer variations.

References

Azetsu-Scott, K., E.P. Jones, I.Yashayaev, and R.M. Gershey, 2003: Time series study of CFC concentrations in the Labrador Sea during deep and shallow convection regimes (1991-2000), *J. Geophys. Res., 108, 11*, 3354, doi:10.1029/2002JC001317.

Beining, P., and W. Roether, 1996: Temporal evolution of CFC 11 and CFC 12 concentrations in the ocean interior, *J. Geophys. Res., 101*, 16455-16464.

Deleersnijder, E., J. Campin, and E. J. M. Delhez, 2001: The concept of age in marine modeling I. Theory and preliminary model results, *J. Mar. Sys., 28*, 229-267.

Dickson B, Yashayaev I, Meincke J, Turrell B, Dye S, Holfort J, 2002: Rapid freshening of the deep North Atlantic Ocean over the past four decades, *Nature, 416*, 832-837.

Doney, S.C., Jenkins, W.J., 1994: Ventilation of the Deep Western Boundary Current and Abyssal Wester North Atlantic: Estimates from tritium and ^{3}He Distributions, *J. Phys. Ocean., 24*, 638-659.

Fine, R.A., Rhein, M., Andrie, C., 2003: Using a CFC effective age to estimate propagation and storage of climate anomalies in the deep western North Atlantic ocean, *Geophys. Res. Lett., 29* (24), 2227, 10.1029/2002GL015618.

Freudenthal S., and Andrie C., 2002: The arrival of a "new" Labrador Sea Water signal in the tropical Atlantic in 1996. *Geophys. Res. Lett., 29*, 1741-1744.

Haine, T.W.N., Watson A.J., Liddicoat M.I., and R.R. Dickson. 1998: The flow of Antarctic bottom water to the southwest Indian Ocean estimated using CFCs *J. Geophys. Res., 103* 27637-27653.

Haine, T. W. N., and T. M. Hall, 2002: A generalized transport theory: Water-mass composition and age, *J. Phys. Oceanogr.*, *32*, 1932-1946.

Hall, T. M., 2000: Path histories and timescales in stratospheric transport: analysis of an idealized model, *J. Geophys. Res., 105*, 22811-22823.

Hall, T. M. and T.W. N. Haine, 2002: A note on ocean transport diagnostics: Ideal age and the age spectrum, *J. Phys. Oceanogr.*, *32*, 1987-1991.

Hall, T. M., and R. A. Plumb, 1994: Age as a diagnostic of stratospheric transport, *J. Geophys. Res.*, *99*, 1059-1070.

Hall, T. M., and D. W. Waugh, 2000: Stratospheric residence time and its relationship to mean age, *J. Geophys. Res.*, *105*, 6773-6782.

Hall, T. M., D. W. Waugh, T. W. N. Haine, P. E. Robbins, and S. Khaliwala, 2004: Reduced estimates of anthropogenic carbon in the Indian Ocean due to mixing and time-varying air-sea CO_2 disequilibrium, *Global Biogeochem. Cycles*, 18, 10.1029/2003GB002120.

Holzer, M., and T. M. Hall, 2000: Transit-time and tracer-age distributions in geophysical flows, *J. Atmos. Sci., 57*, 3539-3558.

Jenkins, W. J., and W. B. Clarke, 1976: The Distribution of 3He in the Western Atlantic Ocean, *Deep-Sea Res., 23*, 481-494.

Johnson H.L., and D.P. Marshall, 2002: Localization of abrupt change in the North Atlantic thermohaline circulation, *Geophys. Res. Lett., 29*, 10.1029/2001GL014140.

Khatiwala, S, M. Visbeck, and P. Schlosser, 2001: Age tracers in an ocean GCM, *Deep-Sea Res., 48,* 1423–1441.

Khatiwala S, Schlosser P, Visbeck M, 2002: Rates and mechanisms of water mass transformation in the Labrador Sea as inferred from tracer observations, *J. Phys. Oceanogr., 32*, 666-686.

Klatt, O, W. Roether, M. Hoppema, K. Bulsiewicz, U. Fleischmann, C. Rodehacke, E. Fahrbach, R. F. Weiss, and J. L. Bullister, 2002. Repeated CFC sections at the Greenwich Meridian in the Weddell Sea, *J. Geophys. Res., 107*, 10.1029/2000JC000731.

Maiss, M., and C. A. M. Brenninkmeijer, 1998: Atmospheric SF_6: Trends, sources, and prospects, *Environ. Sci. Technol.*, *32*, 3077-3086.

Molinari RL, Fine RA, Wilson WD, Curry RG, Abell J, McCartney MS, 1998: The arrival of recently formed Labrador Sea Water in the Deep Western Boundary Current at 26.5 degrees N, *Geophys. Res. Lett., 25*, 2249-2252.

Neu, J. L., and R. A. Plumb, 1999: The Age of Air in "Leaky Pipe" model of Stratospheric Transport, *J. Geophys. Res.*, *104*, 19243-19255.

Pickart R.S., Hogg N.G., Smethie W.M., 1989: Determining the strength of the deep western boundary current using the chlorofluoromethane ratio, *J. Phys. Oceanogr., 19*, 940-951.

Pickart R.S., and Smethie W.M, 1998: Temporal evolution of the deep western boundary current where it enters the sub-tropical domain, *Deep-Sea Res I, 45*, 1053-1083.

Rhein M., 1994: The deep western boundary current - tracers and velocities, *Deep-Sea Res I, 41*, 263-281.

Seshadri V., 1999: *The Inverse Gaussian Distribution*, Springer-Verlag, New York.

Smethie W.M,, and R.A. Fine, 2001: Rates of North Atlantic Deep Water formation calculated from chlorofluorocarbon inventories, *Deep-Sea Res. I*, *48*, 189-215.

Smethie WM, Fine RA, Putzka A, Jones EP, 2000: Tracing the flow of North Atlantic Deep Water using chlorofluorocarbons, *J. Geophys. Res., 105*, 14297-14323.

Sonnerup, R. E., 2001: On the relations among CFC derived water mass ages. *Geophys. Res. Lett, 28*, 1739-1742.

Steinfeldt R., M. Rhein, 2004: Spreading velocities and dilution of North Atlantic Deep Water in the tropical Atlantic based on CFC time series. *J. Geophys. Res., 109*, doi:10.1029/2003JC002050.

Stramma, L, D. Kieke, M. Rhein, F. Schott, I. Yashayaev, and K.P. Koltermann, 2004: Recent Deep Water changes at the western boundary of the subpolar North Atlantic, *Deep-Sea Research I*, to appear.

Walker, S.J., Weiss, R.F., Salameh, P.K, 2000: Reconstructed histories of the annual mean atmospheric mole fractions for the halocarbons CFC-11, CFC-12, CFC-113, and carbon tetrachloride, *J. Geophys. Res., 105*, 14285-14296.

Watts, D.R., 1991: Equatorward currents in temperatures 1.8-6.0C on the continental slope in the Mid-Atlantic Bight, in *Deep Convection and Deep Water Formation in the Ocean*, edited by P.C. Chu and J.C. Gascard, pp.183-196, Elsevier Sci. Publ.

Waugh, D. W., and T. M. Hall, 2002: Age of stratospheric air: Theory, observations, and models, *Rev. Geophys., 40*, 4, 10.1029/2000RG000101.

Waugh, D.W., Hall, T.M., T.W.N. Haine, 2003: Relationships among Tracer Ages, *J. Geophys. Res.*, 108 (5), 10.1029/2002JC001325.

Waugh, D.W., Vollmer M.K., Weiss, R.F., T.W.N. Haine and Hall, T.M., 2002: Transit time distributions in Lake Issyk-Kul, *Geophys. Res. Lett.*, 29 (24), 10.1029/2002GL016201.

Wunsch, C., 2002: Oceanic age and transient tracers: Analytical and numerical solutions, *J. Geophys. Res.*, *107*, 10.1029/2001JC000797.

Yang J., and T.M. Joyce 2003: How do high-latitude North Atlantic climate signals the crossover between the Deep Western Boundary Current and the Gulf Stream *Geophys. Res. Lett., 30*, (2), 10.1029/2002GL015366.

Table 1: Explanation of Symbols

Symbol	**Definition**	**Type**
u	current speed	model parameter
α	ratio of current to interior width	model parameter
t_{mix}	current-interior mixing time	model parameter
$t_{adv} = x/u$	advective time	constrained parameter
$Pe = t_{mix}/t_{adv}$	Peclet number	constrained parameter
Γ	mean transit time	computed diagnostic
σ	standard deviation of TTD	computed diagnostic
T_{exp}	timescale of exponentially increasing tracer	tracer parameter
T_ω	period of periodic tracer	tracer parameter
τ_{exp}	age of exponentially increasing tracer	computed diagnostic
τ_ω	phase lag of periodic tracer	computed diagnostic
A_ω	amplitude of periodic tracer	computed diagnostic

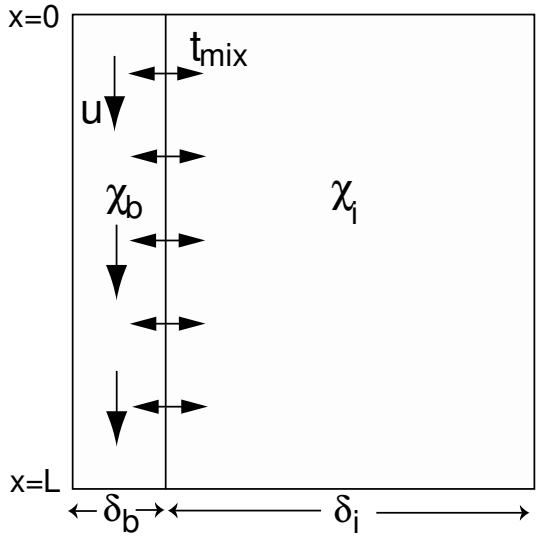

Figure 1: Schematic of boundary current model. The model consists of two regions, a boundary current with width δ_b and uniform flow u, and a larger interior reservoir with width δ_i ($> \delta_b$) and no flow. Mixing between the regions is parameterised as relaxation with timescale t_{mix}. $\chi_b(x,t)$ and $\chi_i(x,t)$ are the tracer concentrations in the boundary current and interior reservoir.

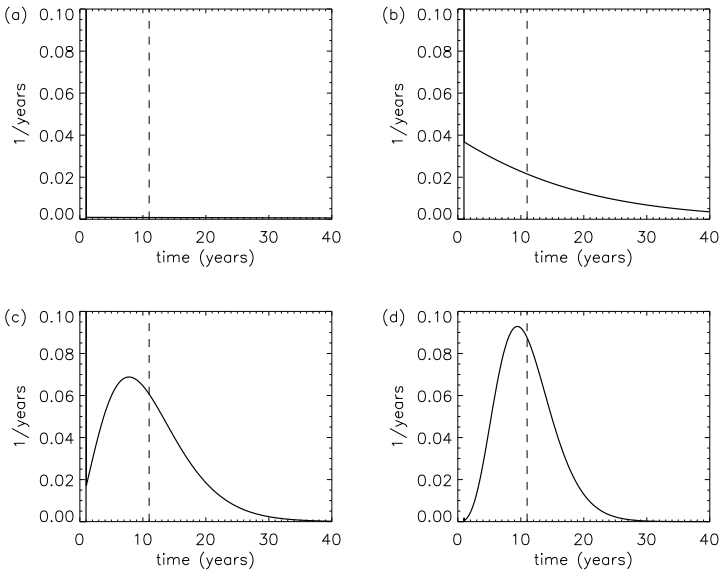

Figure 2: TTDs for DWBC model with fractional boundary current width $\alpha = 0.1$, advective time $t_{adv} = 1$ yr, and mixing time t_{mix} = (a) 10, (b) 1, (c) 0.2, and (d) 0.1 yrs. The vertical dashed lines show the mean transit time Γ.

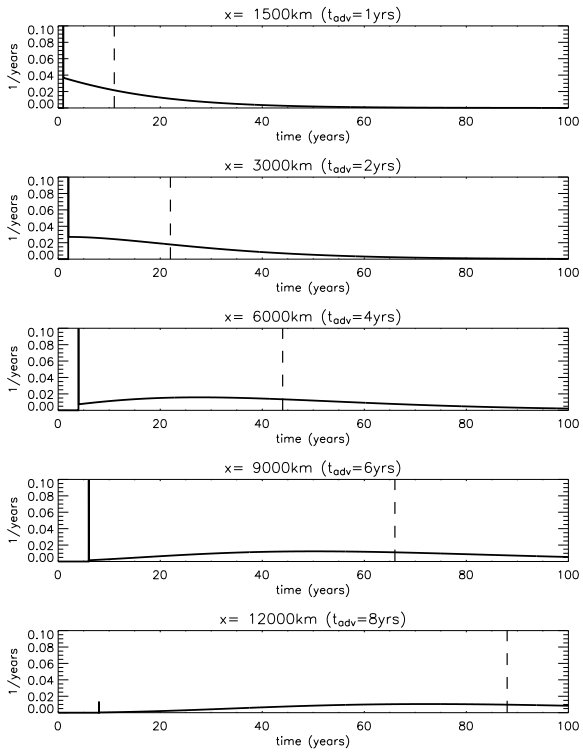

Figure 3: TTDs at a distance x = (a) 1500, (b) 3000, (c) 6000, (d) 9000 and (e) 13500 km downstream from source for $\alpha = 0.1$, $t_{mix} = 1$ yr, and $u = 1500$ km/yr (4.8 cm/s). The advective time t_{adv} to these locations is 1, 2, 4, 6, and 8 yrs, respectively.

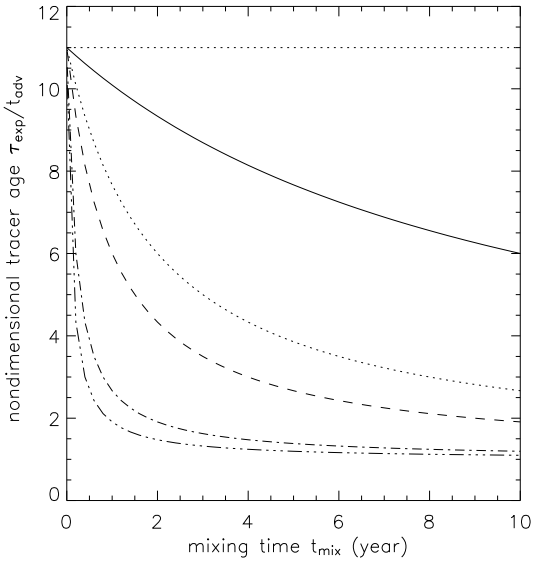

Figure 4: Variation of ratio of age of exponential tracer to advective time τ_{exp}/t_{adv} with mixing time t_{mix}, for tracer growth time $T_{exp} = 100$ (solid curve), 20 (dotted), 10 (dashed), 5 (dot-dashed), and 1 yrs (triple dot-dash). The horizontal dotted line shows the mean transit time Γ .

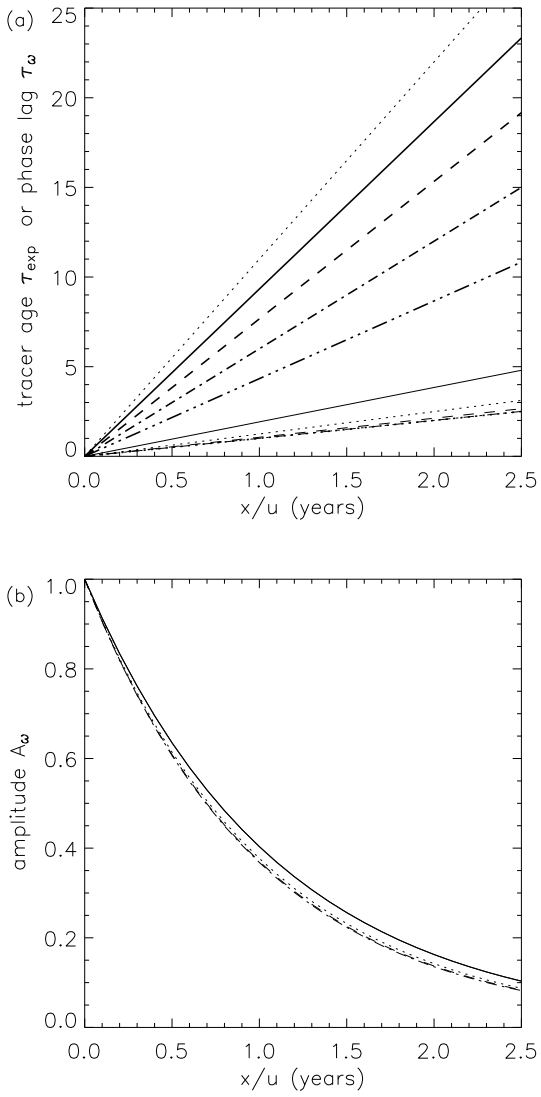

Figure 5: Variation of (a) mean transit time Γ, age of exponential tracer τ_{exp}, and phase lag of periodic tracer τ_ω and (b) amplitude of period tracer A_ω with x/u, for $\alpha = 0.1$ and mixing time $t_{mix} = 1.0$ yr. The upper set of curves in (a) show Γ (dotted curve) and tracer age with $T_{exp} = 50$ (solid curve), 20 (dashed), 10 (dot-dashed), and 5 yrs (triple dot-dash), whereas the lower set of curves show the phase lag for $T_\omega = 20$ (solid), 10 (dotted), 5 (dashed) and 1 (dot-dashed) yrs.

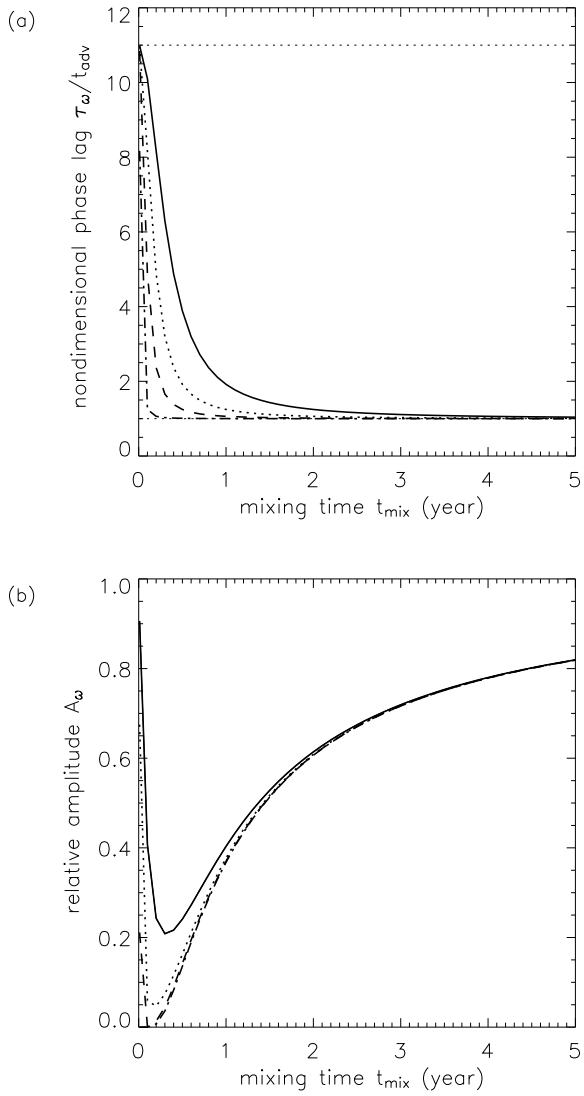

Figure 6: Variation of (a) phase lag τ_ω and (b) amplitude A_ω of periodic tracers with mixing time t_{mix}, for periods equal to 20 (solid curves), 10 (dotted), 5 (dashed) and 1 (dot-dashed) yrs. In both plots $\alpha = 0.1$ and $t_{adv} = 1$ yr.

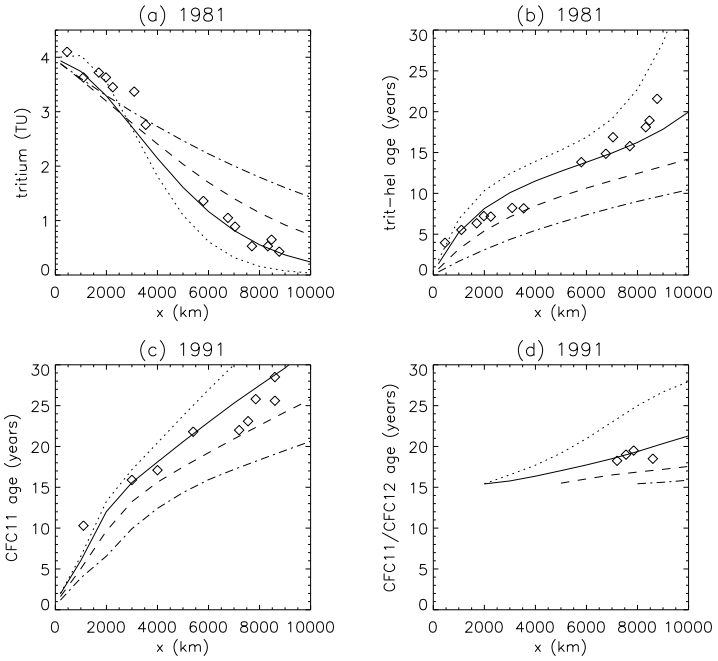

Figure 7: Variation of (a) tritium, (b) tritium-helium age, (c) CFC11 concentration age, and (d) CFC11/CFC12 ratio age with x for $t_{mix} = 4$ (dot-dashed curves), 2 (dashed), 1 (solid) and 0.5 (dotted) yrs. In these calculations $\alpha = 0.1$ and $u = 5$ cm/s ($u = 1575$ km/yr). Tritium concentrations and ages are for 1981, whereas CFC ages are for 1991. Symbols are data from (a,b) Doney and Jenkins (1994) or (c,d) Smethie et al. (2000). See text for details.

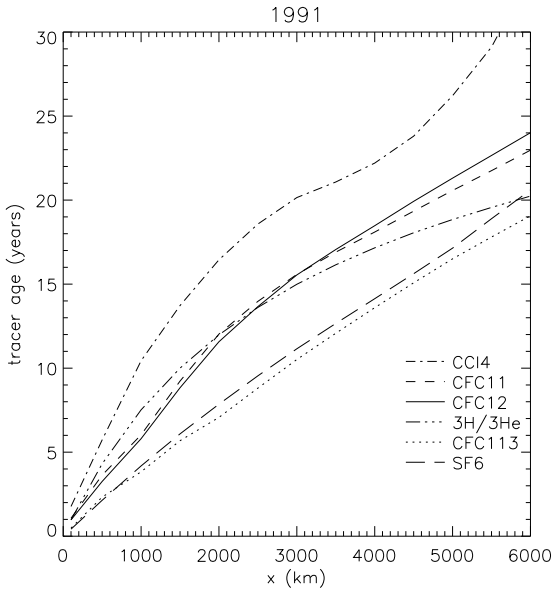

Figure 8: Variation of SF_6 (long dashed curves), CFC113 (dotted), tritium-helium (triple dot -dash), CFC12 (solid), CFC11 (dashed), and CCl_4 (dot-dashed) tracer ages (in 1991) with distance x, for $t_{mix} = 1$ yr, $\alpha = 0.1$ and $u = 5$ cm/s.